Research article

NMR IN BIOMEDICINE

Received: 31 July 2012, Revised: 8 October 2012, Accepted: 9 October 2012, Published online in Wiley Online Library: 28 December 2012

(wileyonlinelibrary.com) DOI: 10.1002/nbm.2887

Exchange-dependent relaxation in the rotating frame for slow and intermediate exchange – modeling off-resonant spin-lock and chemical exchange saturation transfer

Moritz Zaiss* and Peter Bachert

Chemical exchange observed by NMR saturation transfer (CEST) and spin-lock (SL) experiments provide an MRI contrast by indirect detection of exchanging protons. The determination of the relative concentrations and exchange rates is commonly achieved by numerical integration of the Bloch–McConnell equations. We derive an analytical solution of the Bloch–McConnell equations that describes the magnetization of coupled spin populations under radiofrequency irradiation. As CEST and off-resonant SL are equivalent, their steady-state magnetization and dynamics can be predicted by the same single eigenvalue: the longitudinal relaxation rate in the rotating frame $R_{1\rho}$. For the case of slowly exchanging systems, e.g. amide protons, the saturation of the small proton pool is affected by transverse relaxation (R_{2b}). It turns out, that R_{2b} is also significant for intermediate exchange, such as amine- or hydroxyl-exchange or paramagnetic CEST agents, if pools are only partially saturated. We propose a solution for $R_{1\rho}$ that includes R_2 of the exchanging pool by extending existing approaches, and verify it by numerical simulations. With the appropriate projection factors, we obtain an analytical solution for CEST and SL for nonzero R_2 of the exchanging pool, exchange rates in the range 1–10^4 Hz, B_1 from 0.1 to 20 μT and arbitrary chemical shift differences between the exchanging pools, whilst considering the dilution by direct water saturation across the entire Z-spectra. This allows the optimization of irradiation parameters and the quantification of pH-dependent exchange rates and metabolite concentrations. In addition, we propose evaluation methods that correct for concomitant direct saturation effects. It is shown that existing theoretical treatments for CEST are special cases of this approach.

Keywords: spin-lock; magnetization transfer; Bloch–McConnell equations; chemical exchange saturation transfer; PARACEST; hyperCEST

INTRODUCTION

The relaxation of an abundant spin population is affected by a rare spin population owing to inter- and intramolecular magnetization transfer processes mediated by scalar or dipolar couplings or chemical exchange (1). As a consequence, by selective radiofrequency (RF) irradiation of a coupled rare population, not only the relaxation dynamics, but also the steady-state magnetization of the abundant population can be manipulated. As a result of this preparation, the NMR signal of the abundant population contains additional information on the rare population and its interactions. In this context, we analyze two experiments: chemical exchange saturation transfer (CEST) (2) and off-resonant spin-lock (SL).

CEST and SL experiments are commonly applied to enhance the NMR sensitivity of protons in dilute metabolites *in vivo* (3–6), yielding an imaging contrast for different pathologies (7–11). The normalized z magnetization after irradiation at different frequencies, the so-called Z-spectrum, is affected by relaxation and irradiation parameters. In the following, the large pool of water protons is called pool a and the pool of dilute protons pool b. To obtain a pure contrast that depends only on the exchanging pool b, concomitant effects, such as direct water saturation or partial labeling of the exchanging proton pool, must be taken into account in the modeling of Z spectra. Similarities between CEST and SL have been noted previously (12,13). Here, we consider the projection factors that are required for the application of static and dynamic solutions derived for SL to CEST experiments, and vice versa. We demonstrate how the experimental data need to be normalized such that the dynamics of CEST and SL can be described by one single eigenvalue, namely $R_{1\rho}$, the longitudinal relaxation rate in the rotating frame. A first approximation for $R_{1\rho}$ including chemical exchange was published by Trott and Palmer (14). In the present article, this approach is extended by the inclusion of R_{2b}, the transverse relaxation rate of pool b.

An interesting CEST effect is amide proton transfer (APT) of ^{1}H in the backbone of proteins, because quantitative determination of the exchange rate may allow noninvasive pH mapping (15).

* *Correspondence to: M. Zaiss, Department of Medical Physics in Radiology, German Cancer Research Center (DKFZ), Im Neuenheimer Feld 280, 69120 Heidelberg, Germany.*
E-mail: m.zaiss@dkfz.de

M. Zaiss, P. Bachert
Department of Medical Physics in Radiology, German Cancer Research Center (DKFZ), Heidelberg, Germany

Abbreviations used: *APT, amide proton transfer; BM, Bloch–McConnell; CEST, chemical exchange saturation transfer; MT, magnetization transfer; MTR, magnetization transfer ratio; PTR, proton transfer ratio; $R_{1\rho}$, relaxation rate in the rotating frame; RF, radiofrequency; SL, spin-lock.*

The exchange rate k_b for APT is relatively small [$k_b = 28.6 \pm 7.4$ Hz (2)] compared with the transverse relaxation rate of the amide proton pool ($R_{2b} = 1/T_{2b}$). Sun *et al.* (15) measured T_{2b} of 8.5 ms ($R_{2b} = 90.9$ Hz) for amine protons of aqueous creatine at $B_0 = 9.4$ T. For amino protons in ammonium chloride dissolved in agar gel, $T_{2b} = 40$ ms ($R_{2b} = 25$ Hz) was found at $B_0 = 3$ T (16). Thus, R_{2b} in tissue may be in the range of or even surpass k_b and must be taken into account for the quantification of k_b. For systems with strong hierarchy in the eigenvalues – as is the case for diluted spin populations – we present an approximation for $R_{1\rho}$ that includes R_{2b}, and provide an analytical solution for CEST and SL experiments valid for exchange rates in the range of R_{2b}.

THEORY

CEST and SL experiments for coupled spin systems can be described by classical magnetization vectors $\vec{M}$ in Euclidean space governed by the Bloch–McConnell (BM) equations (17). We consider a system of two spin populations: pool *a* (abundant pool) and pool *b* (rare pool) in a static magnetic field $\vec{B}_0 = (0, 0, B_0)$, with forward rate k_b and thermal equilibrium magnetizations $M_{0,a}$ and $M_{0,b}$, respectively. The relative population fraction $M_{0,a}/M_{0,b} = f_b$ is conserved by the back-exchange rate $k_a = f_b k_b$.

The two-pool BM equations are six coupled first-order linear differential equations:

$$\dot{\vec{M}} = \mathbf{A}\cdot\vec{M} + \vec{C}, \quad \mathbf{A} = \begin{bmatrix} \mathbf{L}_a - f_b\mathbf{K} & +\mathbf{K} \\ +f_b\mathbf{K} & \mathbf{L}_b - \mathbf{K} \end{bmatrix} \qquad [1]$$

where ($i = a,b$)

$$\mathbf{L}_i = \begin{pmatrix} -R_{2i} & -\Delta\omega_i & 0 \\ +\Delta\omega_i & -R_{2i} & +\omega_1 \\ 0 & -\omega_1 & -R_{1i} \end{pmatrix}, \quad \mathbf{K} = \begin{pmatrix} k_b & 0 & 0 \\ 0 & k_b & 0 \\ 0 & 0 & k_b \end{pmatrix} \qquad [2]$$

$$\vec{C} = (\quad 0, \quad 0, \quad R_{1a}M_{0,a}, \quad 0, \quad 0, \quad R_{1b}M_{0,b}\ )^{\mathrm{T}} \qquad [3]$$

given in the rotating frame (x,y,z) defined by RF irradiation with frequency ω_{RF}. $\Delta\omega = \Delta\omega_a = \omega_{\mathrm{RF}} - \omega_a$ is the frequency offset relative to the Larmor frequency ω_a of pool *a* (for $^1\mathrm{H}\omega_a / B_0 = \gamma = 267.5$ rad/(μT s)). The offset of pool *b* ($\Delta\omega_b = \omega_{\mathrm{RF}} - \omega_b = \Delta\omega - \delta_b\omega_a$ is shifted by δ_b (chemical shift) relative to the abundant-spin resonance. In contrast with ref. (14), we allow different relaxation rates R_1 and R_2 for the pools. The assumption of their equality is only valid if $|R_{1a} - R_{1b}| \ll k_b$ or $|R_{2a} - R_{2b}| \ll k_b$ (18). Longitudinal relaxation rates $R_{1,a/b} = 1/T_{1,a/b}$ are on the order of a few Hz, whereas transverse relaxation rates $R_{2,a/b} = 1/T_{2,a/b}$ are on the order of 10–100 Hz. For semisolids, R_{2b} can take values up to 10^6 Hz. The RF irradiation field $\vec{B}_1 = (B_1, 0, 0)$ in the rotating frame, with $B_1 \approx \mu\mathrm{T}$, induces a precession of the magnetization with frequency $\omega_1 = \gamma B_1$ around the *x* axis on the order of several 100 rad/s. The population fraction f_b is assumed to be <1%; hence, k_a is 0.01–10 Hz.

Solution of the BM equations for asymmetric populations

The BM equations (Equation [1–3]) are solved in the eigenspace of the matrix **A**, leading to the general solution for the magnetization:

$$\vec{M}(t) = \sum_{n=1}^{6} \mathrm{e}^{\lambda_n t}\ \vec{v}_n + \vec{M}^{ss} \qquad [4]$$

where λ_n is the *n*th eigenvalue with the corresponding eigenvector $\vec{v}_n$ of matrix **A** and $\vec{M}^{ss}$ is the stationary solution. Two eigenvalues are real and four are complex (14). They describe precession and, as all real parts of the eigenvalues are negative, the decay of the magnetization towards the stationary state in each pool. As shown previously (19), if $\Delta\omega$ or ω_1 is large compared with the relaxation rates R_1 and R_2 and the exchange rate k_b, the eigensystem of pool *a* is mainly unaffected. One eigenvector $\vec{v}_1$ is closely aligned with the effective field $\vec{\omega}_{\mathrm{eff}} = (\omega_1, 0, \Delta\omega)$ which defines the longitudinal direction (z_{eff}) in the effective frame (x_{eff},y_{eff},z_{eff}) and is tilted around the *y* axis by the angle $\theta = \tan^{-1}(\omega_1/\Delta\omega)$ off the *z*-axis (Fig. 1a). Mathematical derivation (Appendix A) as well as numerical evaluations (Fig. 1b–d) demonstrate that $\vec{v}_1$ and $\vec{\omega}_{eff}$ are collinear in good approximation if ($R_{2a} - R_{1a}$) is much smaller than ω_{eff}.

The collinearity of the corresponding eigenvector and the effective field is the principal reason why off-resonant SL and CEST exhibit the same dynamics. For an appropriate analysis of a saturation experiment, it is mandatory to identify the initial projections on the eigenvectors and the measured components. $\vec{B}_0$ and $\vec{M}_0$ are parallel to the *z*-axis; the preparation is a projection of the longitudinal magnetization along *z* onto the effective frame:

$$M_{z_{\mathrm{eff}}}(t=0) = cos\theta\cdot M_z(t=0) = P_{z_{\mathrm{eff}}}\cdot M_0 \qquad [5]$$

$$M_{x_{\mathrm{eff}}}(t=0) = sin\theta\cdot M_0; \quad M_{y_{\mathrm{eff}}}(t=0) = 0 \qquad [6]$$

The transverse components induce an oscillation decaying with $T_{2\rho}$ (20), which can be neglected in the case of small θ by averaging over a complete cycle of ω_{eff}, or by measuring after a delay of $5 \cdot T_{2\rho}$. This simplification leads to the relation for the backprojection, via P_z, from z_{eff} to *z*:

$$M_z(t) = cos\theta\cdot M_{z_{\mathrm{eff}}}(t) = P_z\cdot M_{z_{\mathrm{eff}}}(t) \qquad [7]$$

As we identified the effective frame as the eigenspace of the magnetization, Equation [4] can be written as an exponential decay law with the eigenvalue λ_1 associated with the z_{eff} direction. Let the normalized magnetization be $Z = (M_{z,a}/M_{0,a})$ and, for the stationary solution, $Z^{ss} = (M^{ss}_{z,a}/M_{0,a})$. Then, Equation [4], taken for the z_{eff} direction, yields the dynamic solution for the *z* magnetization:

$$Z(\Delta\omega, \omega_1, t) = (P_z P_{z_{\mathrm{eff}}} - Z^{ss})\cdot\mathrm{e}^{\lambda_1\cdot t} + Z^{ss} \qquad [8]$$

Without preparation pulses $P_z = P_{z_{\mathrm{eff}}} \approx cos\theta$ (CEST experiment). If a preparation pulse with flip angle θ is applied before and after continuous wave irradiation, the projection factors are $P_z = P_{z_{\mathrm{eff}}} \approx 1$ (SL experiment); hence, oscillations are suppressed (Fig. 2), but still persist, as z_{eff} is not perfectly collinear with the eigenvector. Transformation of Equation [1] into the effective frame and setting $\frac{\mathrm{d}}{\mathrm{d}t}\vec{M} = 0$ yields the steady-state solution (Appendix A)

$$Z^{ss}(\Delta\omega, \omega_1) = -\frac{P_z\cdot R_{1a}\cdot\cos\theta}{\lambda_1} \qquad [9]$$

It is important to note that, in the case in which the steady state is nonzero, it is locked along the corresponding eigenvector. Equations [8] and [9] agree with the full solution previously found for SL by Jin *et al.* (5), but extend it for CEST.

To obtain a pure dynamic quantity independent of the steady state, we rearrange Equation [8] and define:

NMR IN BIOMEDICINE

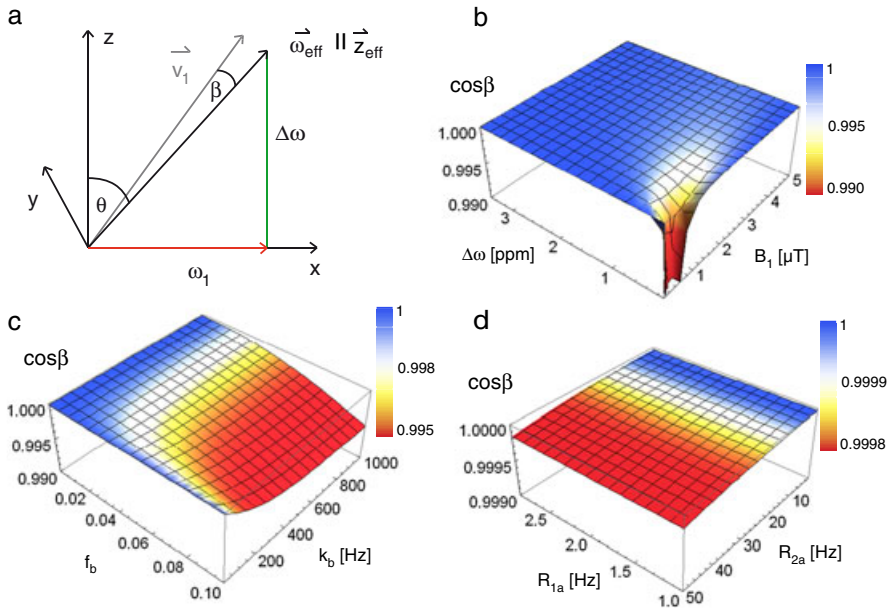

Figure 1. (a) Geometry of the vectors in the rotating frame. (b–d) Cosine of the angle β between the eigenvector of the smallest eigenvalue and $\vec{\omega}_{eff}$. (b) In the far off-resonant case, both vectors are parallel. Near-resonance ω_1 must be strong to keep them parallel. (c) The assumption of collinearity is still valid if pool b with relative concentration $f_b < 10\%$ is coupled to the water pool. (d) Large differences in R_{2a} and R_{1a} lead to an increasing angle between the vectors, but, even for $R_{2a} \approx 50$ Hz and $R_{1a} \approx 1$ Hz, both vectors are still collinear in good approximation. The eigenvector and the effective field vector are collinear if ω_{eff} is large compared with $(R_{2a} - R_{1a})$ (Appendix A) and $f_b < 10\%$ – both are fulfilled for chemical exchange saturation transfer (CEST) experiments, as metabolite concentrations are small and frequency offsets of interest are mostly larger than several 100 rad/s.

$$\tilde{Z}(\Delta\omega, \omega_1, t) \equiv \frac{Z - Z^{ss}}{P_z P_{z_{eff}} - Z^{ss}} = e^{\lambda_1 \cdot t} \qquad [10]$$

Equations [9] and [10] are the central formulae in this article. Actually, the description of SL and CEST experiments differs in the projection factors P_z and $P_{z_{eff}}$. The intuitive solution $Z_{CEST} = \cos\theta \cdot Z_{SL}$ is valid for the steady state, but not for the transient state. If the initial magnetization M_i is not fully relaxed and flipped before the saturation pulse by an angle β, $P_{z_{eff}}$ changes to $\cos(\theta - \beta) \cdot M_i/M_0$.

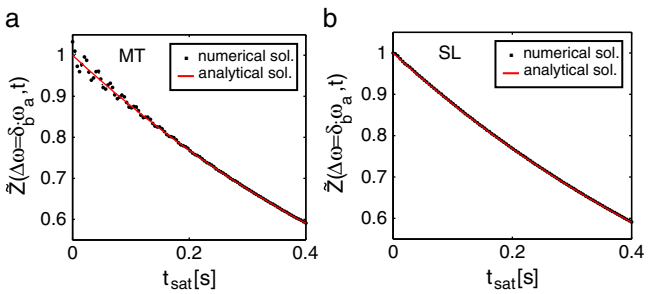

Figure 2. The full numerical Bloch–McConnell (BM) solution (dots) with the proposed normalization (Equation [10]) demonstrates the equivalence of two experiments: (a) chemical exchange saturation transfer (CEST) without preparation pulses; (b) spin-lock (SL) with preparation and measurement in the effective frame. $\tilde{Z}$ of CEST undergoes oscillations because of residual transverse magnetization in the effective frame. SL shows no oscillations as the transverse magnetization in the effective frame is zero ($\Delta\tilde{Z} = 0$, see text) (Equation [24]). Both SL and CEST show the same monoexponential decay of the z magnetization with λ_1 (Equation [14]) (full red line). For full BM simulations (21), parameters were taken from the amide proton system (3) in brain white matter (22) at $B_0 = 3$ T. If not varied, $R_{2a} = 14.5$ Hz, $R_{1a} = R_{1b} = 0.954$ Hz, $R_{2b} = 66.6$ Hz, $f_b = 1\%$, $k_b = 25$ Hz, $\delta_b = 3.5$ ppm, $B_1 = 1$ μT, $t_{sat} = 1$ s.

After obtaining an understanding of the transition between the two experiments, we now solve the dynamics of CEST and SL experiments by finding the corresponding eigenvalue and verify it numerically.

As already demonstrated for the SL experiment (14), the eigenvalue, which corresponds to the eigenvector along the z_{eff} axis, is the smallest eigenvalue in the modulus of the system. Assuming that all eigenvalues of an arbitrary full-rank matrix **A** are much larger in modulus than the smallest eigenvalue, i.e. $|\lambda_1| \ll |\lambda_{2,\ldots,n}|$, we obtain (see Appendix B):

$$\lambda_1 \approx -\frac{c_0}{c_1} \qquad [11]$$

where c_0 and c_1 are the coefficients of the constant and the linear term of the normalized characteristic polynomial, respectively. We derive the full solution for the smallest eigenvalue by employing the solution of the unperturbed system ($f_b = 0$). The solution is $\lambda_{eff} = -R_{eff}$, with the decay rate in the effective frame R_{eff}, which was shown to be approximately (19):

$$-R_{eff} = R_{1a}cos^2\theta + R_{2a}sin^2\theta \qquad [12]$$

With this eigenvalue of the unperturbed system, we can rescale the system by:

$$\mathbf{A}' = \mathbf{A} - \mathbf{I} \cdot \lambda_{eff} \qquad [13]$$

thus shifting the smallest eigenvalue by R_{eff}. The smallest eigenvalue of $\mathbf{A}'$ still contains terms of R_{1a} and R_{2a}, but represents the exchange-induced perturbation of $R_{1\rho}$.

The result is a strong hierarchy (Fig. 3) in the eigenvalues of **A**′ if the coupling is small ($f_b \ll 1$). Now Equation [11] can be employed to calculate the eigenvalue $\lambda_1{}'$ of the matrix **A**′ to obtain the full solution:

$$\lambda_1 = \lambda_{\text{eff}} + \lambda_1{}' \qquad [14]$$

Here $\lambda_1{}' = -c_0{}'/c_1{}'$ is the ratio of the coefficients of the characteristic polynomial of the matrix **A**′. This analytical procedure gives a very good approximation of the dynamics of the BM system.

For further simplification, we assume that relaxation of pool *a* is well described by R_{eff} and the perturbation is dominated by the exchange and relaxation of pool *b*. We call the exchange-dependent relaxation rate $R_{\text{ex}} = -\lambda_1{}'$. The eigenvalue λ_1 is associated with z_{eff} and is therefore an approximation of the relaxation rate in the rotating frame $R_{1\rho} \approx -\lambda_1$ given by Equations [12] and [14]:

$$R_{1\rho}(\Delta\omega) = R_{\text{eff}}(\Delta\omega) + R_{ex}(\Delta\omega) \qquad [15]$$

To derive a useful approximation of R_{ex}, we neglect all relaxation terms of pool *a* in matrix **A**′. Furthermore, we assume that R_{1b} is much smaller than R_{2b} and k_b, and therefore R_{1b} can be neglected in **A**′. In contrast with Trott and Palmer (14), we do not neglect R_{2b}, but k_a. By this means, the obtained eigenvalue approximation using Equation [11] is linearized in the small parameter f_b giving:

$$R_{\text{ex}}(\Delta\omega_b) = \frac{R_{\text{ex}}^{\max}\frac{\Gamma^2}{4}}{\frac{\Gamma^2}{4} + \Delta\omega_b^2} \qquad [16]$$

with maximum value:

$$R_{\text{ex}}^{\max} = f_b k_b \sin^2\theta \frac{(\omega_a - \omega_b)^2 + \frac{R_{2b}}{k_b}\left(\omega_1^2 + \Delta\omega^2\right) + R_{2b}(k_b + R_{2b})}{\frac{\Gamma^2}{4}} \qquad [17]$$

and full width at half-maximum:

$$\Gamma = 2\sqrt{\frac{k_b + R_{2b}}{k_b}\omega_1^2 + (k_b + R_{2b})^2} \qquad [18]$$

For large $|\omega_b - \omega_a|$:

$$R_{\text{ex}}^{\max} \approx f_b k_b \cdot \frac{\omega_1^2}{\omega_1^2 + k_b(k_b + R_{2b})}. \qquad [19]$$

The ω_1-dependent factor yields the amount of labeling of pool *b*. Hence, we call this factor the labeling efficiency, referring to (23):

$$\alpha = \frac{\omega_1^2}{\omega_1^2 + k_b(k_b + R_{2b})} \qquad [20]$$

For strong B_1 and small R_{2b} and k_b, α is approximately unity, and we obtain the full-saturation limit:

$$R_{\text{ex}}^{\max} \approx f_b k_b = k_a \qquad [21]$$

RESULTS

We obtained numerical values for the eigenvalues computed by means of the full numerical BM matrix solution (21) and compared them with the proposed approximations via:

$$R_{\text{ex}} = -\left|\lambda_{1,\text{numerical}}\right| - R_{\text{eff}}. \qquad [22]$$

To verify Equations [9], [10], [14] and [17], the dynamics of the magnetization vectors of the exchanging spin pools were simulated. The decay rate R_{ex} is obtained from $\tilde{Z}$ (Equation [10]) and R_{eff} via:

$$R_{\text{ex}} = -\frac{log(\tilde{Z})}{t_{\text{sat}}} - R_{\text{eff}}. \qquad [23]$$

The simulation parameters for the abundant pool were chosen according to published data for brain white matter (22), including a rare pool attributed to amide protons (2).

The proposed approximation of R_{ex} by Equation [16] was compared with the asymmetric population solution of ref. (14) (Fig. 4). If R_{2b} is nonzero, R_{ex} proposed by Equation [16] matches the numerical value better than does R_{ex} given in ref. (14) (see

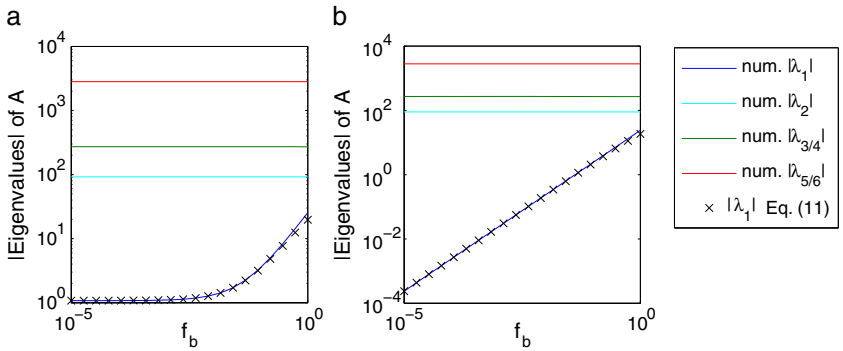

Figure 3. Hierarchy of numerically calculated Bloch–McConnell (BM) eigenvalues (lines) of the standard system (see Fig. 2). The rescaled matrix **A**′ (Equation [13]) (b) has a much stronger hierarchy in the eigenvalues than does matrix **A** (a). This improves the approximation of the smallest eigenvalue (*x*, Equation [11]).

NMR IN BIOMEDICINE

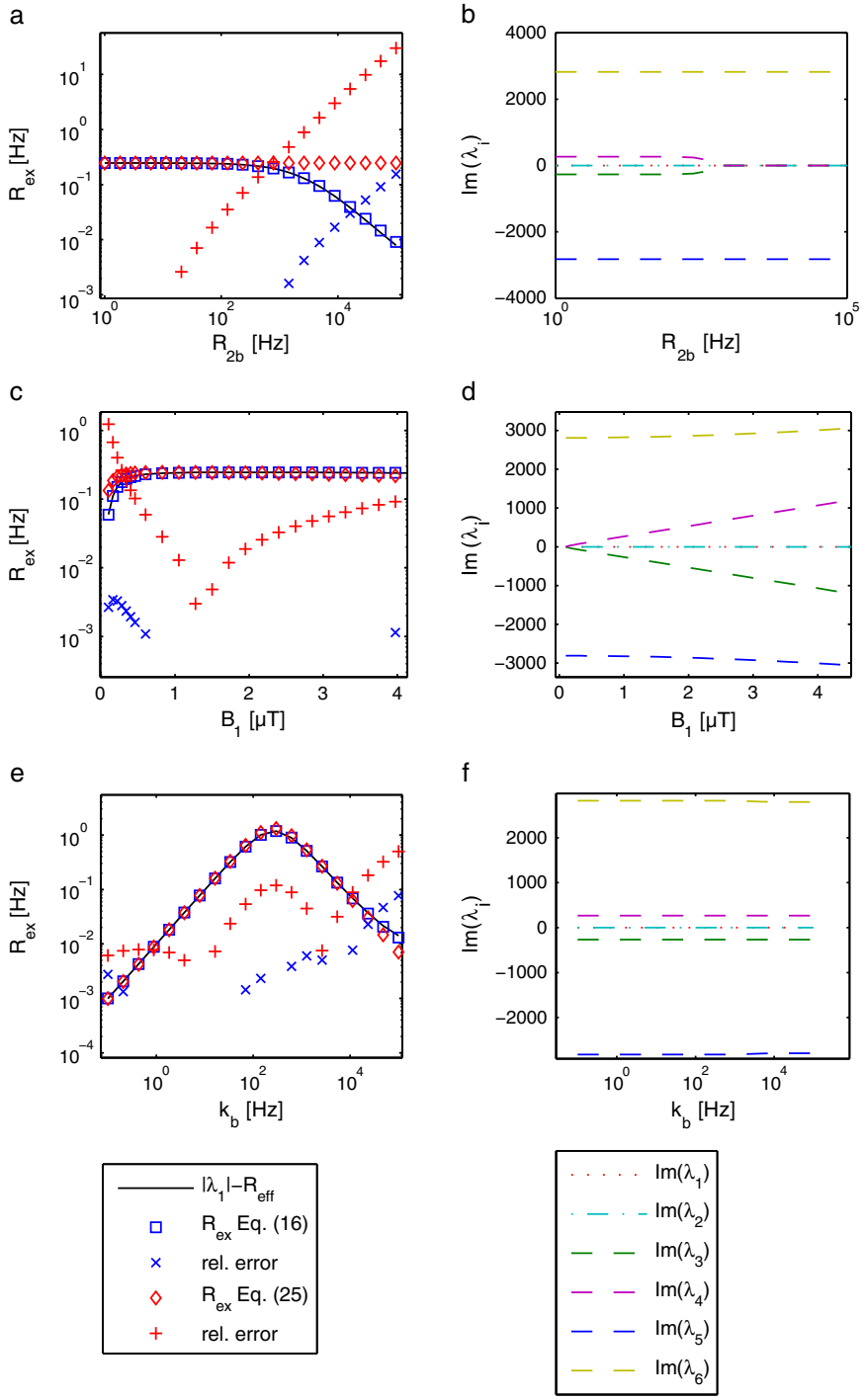

Figure 4. (a,c,e) R_{ex} for the case of $\Delta\omega_b = 0$ (on-resonant irradiation on pool *b*) from smallest eigenvalue in modulus (Equation [22]), calculated numerically (line) and analytically by the approximations of Equation [16] (squares) and the asymmetric population limit of Trott and Palmer (14) (Equation [25], diamonds). '×' and '+' mark the relative error [1 – ($R_{ex}^{ana}/R_{ex}^{num}$)] when it is larger than 0.1%. (a) For small R_{2b}, both solutions for R_{ex} agree with the numerical value; if R_{2b} is larger than k_b, the proposed solution still matches the numerical value. The extension by R_{2b} is important if the metabolite pool (pool *b*) is not fully saturated, which is the case for small B_1 (c) or large k_b (e). For large B_1, the solution that includes R_{2b} fits the numerical value with higher accuracy. (b,d,f) Imaginary parts of the numerical eigenvalues. B_1 and R_{2b} ranges, in which Equation [16] (squares) yields deviations from the numerical solution, correlate with ranges in which the imaginary part becomes small or even zero. In this case, the assumption of a strong hierarchy in the eigenvalues is no longer valid.

Equation [25] below). In particular, the modeling of the dependence of R_{ex} on B_1 (Fig. 4c) is improved by taking R_{2b} into account.

For a CEST experiment, the normalized numerical solution agrees with the theory of dynamic $\tilde{Z}$ spectra (Fig. 5a, b) and steady-state *Z* spectra (Fig. 5c, d) for different values of B_1 and

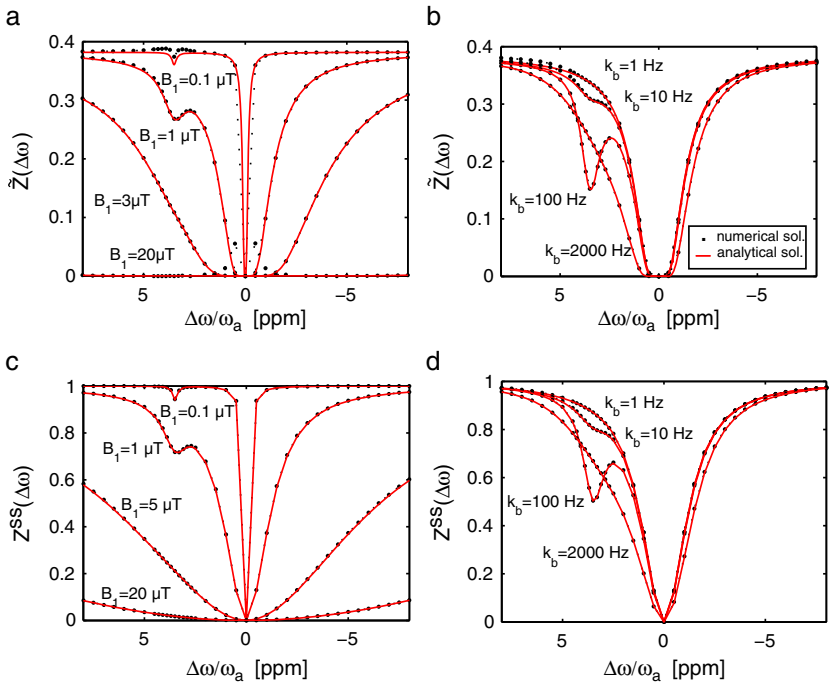

Figure 5. Numerical simulations (dots) of a chemical exchange saturation transfer (CEST) experiment evaluated for dynamic $\tilde{Z}$-spectra (a, b) and steady-state Z-spectra (c, d) are in agreement with Equations [10] and [9] (full red lines), respectively. Plots demonstrate high correlation for different B_1 (0.1–20 μT; a,c) and k_b (1–2000 Hz; b,d). Deviations near resonance of pool a for large B_1 (a) are caused by oscillations of the magnetization in the transverse plane of the effective frame. In the spin-lock (SL) experiment, these oscillations are suppressed (Fig. 2).

k_b. The competing direct and exchange-dependent saturation – a central problem in proton CEST (15,23,24) – is modeled correctly. Deviations in Figure 5a for strong B_1 and $\Delta\omega \to 0$ result from transverse magnetization in the effective frame, which was neglected previously. By projection on the transverse plane of the effective frame using Equation [6], we obtain the resulting deviation of $\tilde{Z}$:

$$\Delta\tilde{Z}(\Delta\omega,\omega_1,t) = \frac{P_x P_{x_{\text{eff}}}}{P_z P_{z_{\text{eff}}} - Z_{\text{ss}}} \cdot \text{Re}\left(e^{\lambda_2 \cdot t}\right) \qquad [24]$$

with projections $P_{x_{\text{eff}}}$ and P_x into the transverse plane of the effective frame and back. For MT, $P_x = P_{x_{\text{eff}}} = sin\theta$. Real and imaginary parts of the complex eigenvalue λ_2 are given by $-R_{2\rho} \approx -\frac{1}{2}(R_{2a} + R_{1a}sin^2\theta + R_{2a}cos^2\theta)$ (20) and ω_{eff}, respectively. The implicit neglect of $\Delta\tilde{Z}$ in Equation [10] is justified if $t_{\text{sat}} \gg T_{2\rho}$ or P_x and $P_{x_{\text{eff}}}$ are small. This can be realized either by SL preparation or by $\omega_1 \ll \Delta\omega$. The on-resonant case of CEST ($\theta = 90°$) is not defined, because Z^{ss} in Equation [9] and thus the denominators in Equations [10] and [24] vanish. Then, the z axis lies in the transverse plane of the effective frame and Z is described by $M_{0,a} \cdot Re\left(e^{\left(-\left(R_{2\rho}+i\omega_1\right)t\right)}\right)$. Therefore, near-resonance SL is preferable to CEST; it also yields, in general, a higher signal-to-noise ratio (given by the projection factors P_z, $P_{z_{\text{eff}}}$). With regard to the experimental realization, CEST is simpler than SL, because $\Delta\omega$ and ω_1, and thus θ, can be corrected effectively after the measurement by B_0 and B_1 field mapping (23,25). In contrast, SL requires a knowledge of B_1 and B_0 during the scan for appropriate preparation or techniques that are insensitive to field inhomogeneities, such as adiabatic pulses (26,27).

The values of the rate $R_{\text{ex}}^{\text{max}}$ obtained by the simulations fit well with the full (Equation [14]) and approximate (Equation [17]) solutions for the observed parameters (Fig. 6). Deviations between simulation and analytical solution were smaller than 1% for rate variations in the range: $R_{1b} = 0.1$–10 Hz, $R_{1a} = 0.1$–10 Hz and $R_{2a} = 2$–100 Hz (data not shown).

DISCUSSION

General solution

We showed that our formalism, established by Equations [8]–[10], together with the eigenvalue approximation of Equation [14], is a general solution for CEST experiments. This now allows us to discuss, from a general point of view, the techniques and theories proposed in the field of CEST. For the SL solution, this has already been accomplished by Jin *et al.* (5,12).

The proposed eigenvalue approximation assumes the case of asymmetric populations. This restricts its application to systems in which the water proton pool is much larger than the exchanging pools – which is the case for CEST experiments. There are many analytical approaches for the smallest eigenvalue ($R_{1\rho}$) of the BM matrix in addition to our approach. They use pertubation theory (19), the stochastic Liouville equation (28), an average magnetization approach (29) and the polynomial root finding algorithm of Laguerre (18). The latter is even valid in the case of symmetric populations. However, all of these treatments neglect the transverse relaxation of the exchanging pool. As, in CEST experiments, the exchange rates are often quite small (e.g. $k_b \approx 28$ Hz for APT), R_{2b} cannot be neglected against k_b. Therefore, we chose a simple approach which is suitable for the condition of asymmetric populations and took R_{2b} into account. Our approach to find the eigenvalue including R_{2b} is similar to that of Trott and Palmer (14). However, different R_1 and R_2 were allowed for the involved pools. In addition, an alternative justification of the relation $\lambda_1 = -(c_0/c_1)$ was

NMR IN BIOMEDICINE

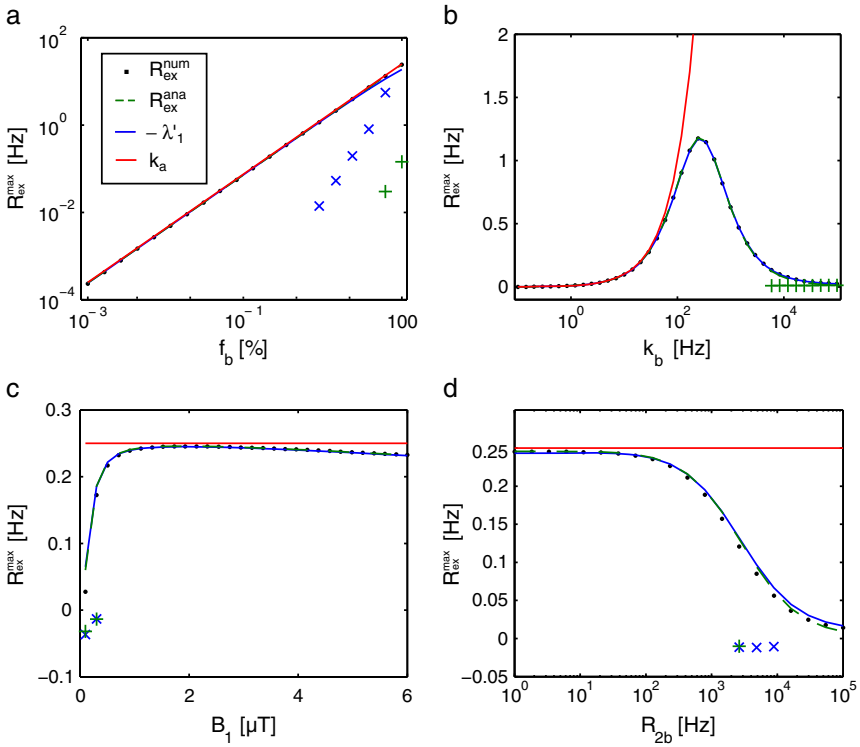

Figure 6. Numerical R_{ex}^{max} (dots), employing Equation [23], fitted to $-\lambda_1'$ of Equation [14] (full blue lines) and to R_{ex}^{max} of Equation [17] (broken green lines) as a function of f_b, k_b, B_1 and R_{2b}. '×' and '+' mark the relative error [1 – ($R_{ex}^{ana}/R_{ex}^{num}$)] when it is larger than 1%. (a) As expected, the eigenvalue approximation is insufficient for $f_b > 5\%$. (b) Contrary to the approximation of Equation [21] (full red lines), the full solution follows the decrease in R_{ex}^{max} with large k_b. The decrease in deviations for small B_1 (c) and high R_{2b} (d) may be caused by overdamping in pool *b*, i.e. eigenvalues become real, which reduces the required hierarchy in the set of eigenvalues. However, the deviation in R_{ex} is too small (Fig. 4) to explain this deviation, leading to the conclusion that other eigenvectors are contributing to the relaxation. (d) Inclusion of R_{2b} is relevant for $R_{2b} > 100$ Hz.

obtained, which uses the intrinsic hierarchy of the eigenvalues (Appendix B) instead of linearization of the characteristic polynomial. By this means, it was shown that a strong hierarchy of the eigenvalues is necessary for the approximation. The hierarchy was increased by rescaling the system by the unperturbed eigenvalue R_{eff} (Fig. 3). Thus, the accuracy of the approximation was improved. As the parameter R_{2b} was included and equations were linearized directly in the small parameter k_a, a formula was obtained (Equation [15]) that differs from the asymmetric population limit of ref. (14) reading:

$$R_{1\rho} = R_{eff} + \underbrace{sin^2\theta \frac{(\omega_b - \omega_a)^2 \frac{k_a k_b}{k_a + k_b}}{\Delta\omega_b^2 + \omega_1^2 + (k_a + k_b)^2}}_{R_{ex}} \qquad [25]$$

Equality is reached if R_{2b} is neglected in our approximation and if Equation [25] is linearized in k_a. With our extension, simulated CEST *Z* spectra could be predicted well with a broad range of parameters. Moreover, it was shown that R_{2b} is important if it is in the range of k_b (Fig. 6d). Inclusion of R_{2b} also allows the modeling of macromolecular magnetization transfer effects with large R_{2b} values (Fig. 8c).

Our solution agrees for SL with the existing treatment (12), but only with the correct projection factors can SL and CEST be described by the same theory. This is contrary to the conclusion of Jin *et al.* (12) that SL theory can be used directly to describe CEST experiments. The deviation is not large for small θ, but, for $\omega_1 \approx \Delta\omega$, the projection factors are crucial, as shown in Figure 7.

With the correct projections, the transition to CEST is straightforward and provides a much broader range of validity than previous models developed for CEST which are either appropriate only for small B_1 (24) or large B_1 (30), or only for the case of on-resonant irradiation of pool *b* (15,23). The proposed theory (Equation [8]) gives a model for full *Z*-spectra for transient and steady-state CEST experiments which enables analytical rather than numerical fitting of the experimental data.

Extension to other systems

As verified for SL (19), the theory can be extended to *n*-site exchanging systems. By simply superimposing the exchange-dependent relaxation rates of several pools, one obtains the *Z*-spectra for a multi-pool system. We applied this to the contrast agent iopamidol in water, which has two exchanging amide proton groups (31), considering a three-pool system: water, amide proton B at 4.2 ppm and amide proton C at 5.5 ppm. Assuming for the exchange rates $k_c = 6k_b$, the superposition of R_{eff} and the two corresponding R_{ex} yields the *Z* spectrum of the iopamidol system (Fig. 8a). A three-pool system relevant for *in vivo* CEST studies includes water protons, amide protons and a macromolecular proton pool. Modeling the macromolecular pool by R_{ex}^{m} ($R_{2m} = 5000$ Hz, $k_m = 40$ Hz) with an offset of -2.6 ppm, and again superimposing it with R_{ex}^{amide}, we are able to model analytically the *Z*-spectra of APT with an underlying symmetric and asymmetric MT effect up to 5% relative concentration f_m (Fig. 8b). Hence, the model is able to describe the *in vivo* situation of several CEST pools and underlying MT competing with direct water saturation. Using the superimposed R_{ex}, including R_{ex}^{m} and R_{ex}^{amide}, and fitting the obtained *Z*-spectra,

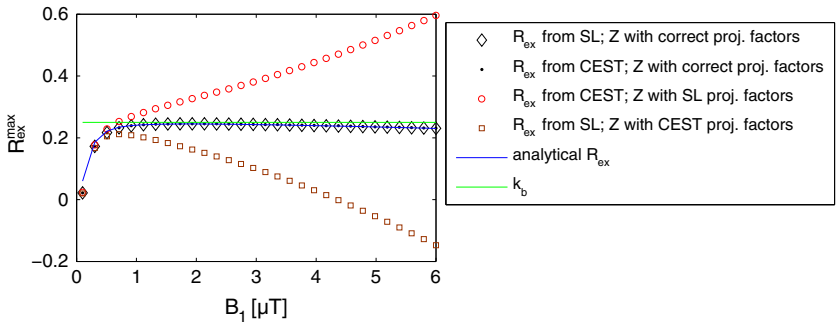

Figure 7. The same plot of R_{ex}^{max} (Equation [23]) as in Fig. 6c, but for chemical exchange saturation transfer (CEST) (dots) and spin-lock (SL) (diamonds) employing the corresponding projection factors in Equation [10] ($P_z = P_{z_{eff}} = 1$ for SL and $P_z = P_{z_{eff}} = cos\theta$ for CEST). In addition, the result of an evaluation is shown employing the projection factors of SL for a CEST experiment (circles) and the projection factors of CEST for an SL experiment (squares). Only with the correct projection factors are both experiments described by the same theory and yield R_{ex} (full blue line).

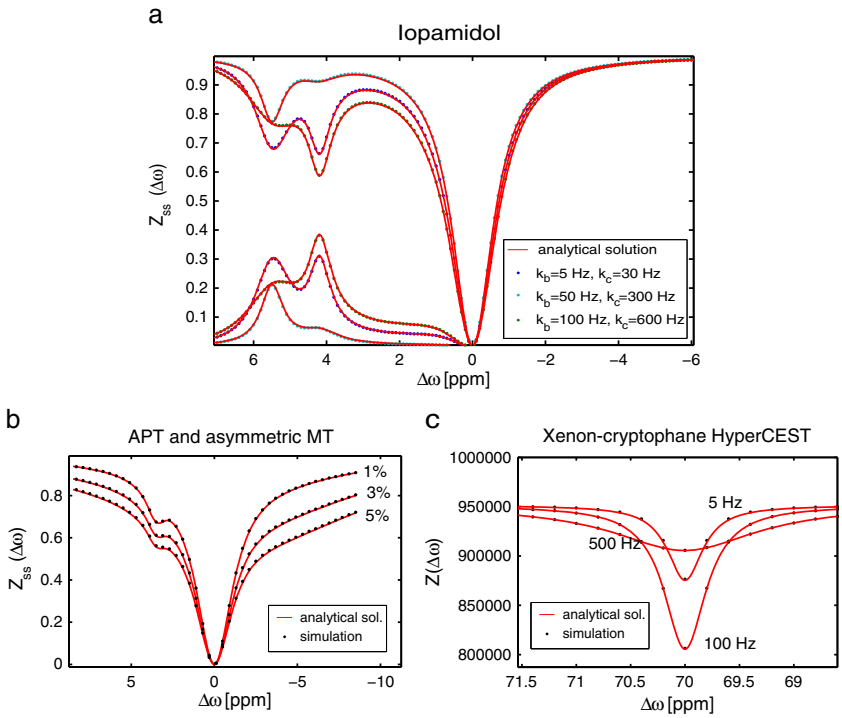

Figure 8. Three applications of the proposed theory: (a) system of iopamidol with corresponding asymmetric magnetization transfer ratio (MTR_{asym}) evaluation; (b) system of amide proton transfer (APT) with an asymmetric macromolecular magnetization transfer (MT) pool (for concentration fractions $f_m = 1\%$, 3% and 5%); (c) system of exchanging hyperpolarized xenon dissolved or encapsulated in cryptophane cages, a biosensor method called HyperCEST.

R_{ex}^{amide} can be isolated. For macromolecular MT, the extension of R_{ex} by R_{2b} is crucial, as R_{2b} can be as large as $\approx 10^5$ Hz. The implicitly assumed Lorentzian lineshape of the macromolecular pool is only valid around the water proton resonance; for large offsets, a super-Lorentzian lineshape must be included in R_{ex}^{m} (22).

Hyperpolarized xenon spin ensembles exchanging between the dissolved phase and cryptophane cages [HyperCEST experiment (32)] can also be described by Equation [10]. As the initial hyperpolarized magnetization M_i is on the order of up to 10^5–10^6 M_0, the steady state can be neglected for depolarization. This yields $Z \approx \tilde{Z} = M_i \cdot e^{-R_{1\rho} t_{sat}}$, in agreement with the result in ref. (33). Figure 8c shows the simulated Z spectrum around the cage peak in the HyperCEST experiment of a xenon–cryptophane system for different k_b.

Pulsed irradiation, employed for saturation in SAR-limited clinical scanners (34), has been shown to have similar effects on the asymmetric magnetization transfer ratio (MTR_{asym}) as continuous wave irradiation with effective B_1 (35,36). The presented solution for CEST Z spectra can therefore be used for the optimization of pulsed saturation transfer experiments.

Proton transfer ratio (PTR)

For a CEST experiment, the parameters of particular interest are the exchange rate k_b of the metabolite proton pool and the relative concentration f_b. The former is often pH catalyzed and permits pH-weighted imaging; the latter allows molecular imaging with enhanced sensitivity. The ultimate method must

allow – with high spectral selectivity – the generation of k_b and f_b maps separately and for different exchanging groups. Unfortunately, both parameters occur in the water pool BM equations as a product, i.e. the back-exchange rate $k_a = k_b f_b$. There are some approaches which are able to separate k_b and f_b for specific cases, such as rotation transfer of amide protons (37) or the method of Dixon *et al.* (38) applicable to PARACEST agents. CEST experiments are commonly evaluated to yield the PTR. PTR is an ideal parameter in the sense that it reflects the decrease in the water pool signal owing to exchange from a labeled exchanging pool only, thus neglecting any direct saturation.

In the following, we assume one CEST pool resonance on the positive $\Delta\omega$ axis.

Employing Equation [9] with the limit $\theta \to 0$, we obtain for PTR in steady state:

$$\mathrm{PTR} = 1 - Z^{ss}(\Delta\omega) \approx \frac{R_{ex}(+\Delta\omega)}{R_{1a} + R_{ex}(+\Delta\omega)} \qquad [26]$$

which yields the maximal value $k_a/(R_{1a}+k_a)$ (2) in the full-saturation limit ($R_{ex} \approx k_a$). Equation [26] is consistent with PTR including the labeling efficiency α introduced in ref. (23).

Z spectra evaluation – MTR and MTR_{asym}

Methods using asymmetry implicitly assume that the full width at half-maximum of R_{ex} ($\Delta\omega_b$) is narrow compared with the chemical shift of the corresponding pool. This means that R_{ex} ($\Delta\omega_b$) can be neglected for the reference scan $Z(-\Delta\omega)$, which is only true in the slow exchange limit (2). This limit can be defined more generally by the width of R_{ex} ($\Delta\omega_b$) (Equation [18]):

$$\Gamma = 2\sqrt{\frac{k_b + R_{2b}}{k_b}\cdot\omega_1^2 + (k_b + R_{2b})^2} \ll |\Delta\omega_b - \Delta\omega_a| \qquad [27]$$

This new limit depends on B_1 which affects the ability to distinguish different peaks in the Z spectrum (Fig. 5c). The limit is therefore a useful parameter for exchange regime characterization in saturation spectroscopy.

For CEST, the common evaluation parameters are $\mathrm{MTR}(\Delta\omega) = 1 - Z(\Delta\omega)$ and the asymmetry of the Z spectrum $\mathrm{MTR}_{asym}(\Delta\omega) = Z(-\Delta\omega) - Z(+\Delta\omega)$. MTR_{asym} is generally employed to estimate PTR. Using Equation [9] together with Equation [15], we obtain, for steady-state Z-spectrum asymmetry:

$$\begin{aligned}\mathrm{MTR}^{ss}_{asym}(\Delta\omega) &= Z^{ss}(-\Delta\omega) - Z^{ss}(+\Delta\omega) \\ &= \frac{(R_{ex}(+\Delta\omega) - R_{ex}(-\Delta\omega))\cdot R_{1a} P_z \cos\theta}{(R_{eff} + R_{ex}(-\Delta\omega))(R_{eff} + R_{ex}(+\Delta\omega))}\end{aligned} \qquad [28]$$

The comparison shows that MTR^{ss}_{asym} yields PTR of Equation [26] only if $\theta = 0$.

Sun *et al.* (15) suggested $\mathrm{MTR}^{ss}_{asym} = \mathrm{PTR}\cdot\alpha\cdot(1-\sigma)$, which combines the labeling efficiency α obtained by the weak saturation pulse approximation and a spillover coefficient σ from the strong saturation pulse approximation. This formula is only valid on resonance of pool b in contrast with Equation [28].

Another approach, applicable for small B_1, eliminates the spillover effect by a probabilistic approach (24). This Z spectrum model taken from ref. (24) yields:

$$\begin{aligned}\mathrm{PTR}(\Delta\omega) &\approx \frac{Z^{ss}(-\Delta\omega) - Z^{ss}(+\Delta\omega)}{Z^{ss}(-\Delta\omega) - Z^{ss}(+\Delta\omega) + Z^{ss}(-\Delta\omega)\cdot Z^{ss}(+\Delta\omega)} \\ &= \frac{R_{ex}(+\Delta\omega)}{\cos^2\theta\cdot R_{1a} + R_{ex}(+\Delta\omega)}\end{aligned} \qquad [29]$$

which, after substitution of Z^{ss} by Equation [9], is an approximation of PTR if θ is small. Important to note is that Equation [29] does not depend on R_{eff}. The asymmetry normalized by the reference scan was proposed for spillover correction (39). Application of Equation [9] yields:

$$\frac{Z^{ss}(-\Delta\omega) - Z^{ss}(+\Delta\omega)}{Z^{ss}(-\Delta\omega)} = \frac{R_{ex}(+\Delta\omega)}{R_{eff}(+\Delta\omega) + R_{ex}(+\Delta\omega)} \qquad [30]$$

which again approximates PTR if θ is small.

By the use of Equations [8] and [9], we obtain for the asymmetry in the transient state, a biexponential function:

$$\begin{aligned}\mathrm{MTR}_{asym}(\Delta\omega, t) &= \mathrm{MTR}^{ss}_{asym}(\Delta\omega) \\ &+ e^{-R_{1\rho}(-\Delta\omega)t}\cdot(P_z P_{z_{eff}} - Z^{ss}(-\Delta\omega)) \\ &- e^{-R_{1\rho}(+\Delta\omega)t}\cdot(P_z P_{z_{eff}} - Z^{ss}(+\Delta\omega))\end{aligned} \qquad [31]$$

Neglecting direct saturation of pool a and assuming $P_z = P_{z_{eff}} = 1$ yields the monoexponential approximation at the CEST resonance (2,40):

$$\mathrm{MTR}_{asym}(\Delta\omega_b = 0, t) = \mathrm{MTR}^{ss}_{asym}(\Delta\omega_b = 0)\cdot\left(1 - e^{-(R_{1a}+k_a)t}\right) \qquad [32]$$

with the rate constant $R_{1\rho} = R_{1a} + k_a$. This is valid if θ is small, leading to $R_{eff} \approx R_{1a}$, and, with the limit of Equation (21), $R_{ex} \approx k_a$ (full red line, Fig. 6b).

The ratiometric analysis approach QUESTRA (41) includes direct saturation and is independent of the steady state. It can be expressed by means of Equation [10] under the same assumptions $P_z = P_{z_{eff}} = 1$, and $R_{eff} \approx R_{1a}$ and $R_{ex} \approx k_a$:

$$\mathrm{QUESTRA}(t) = \frac{\tilde{Z}(+\Delta\omega, t)}{\tilde{Z}(-\Delta\omega, t)} \approx e^{-k_a t}. \qquad [33]$$

Another method, pCEST (13), employs $R_{1\rho}$ in an inversion recovery experiment. The pCEST signal obeys the negative of Equation [31] if the initial inversion is introduced by $P_{z_{eff}} = -\cos\theta$. Hence, the full dynamics of the $R_{1\rho}$ inversion recovery signal is:

$$\mathrm{pCEST}(\Delta\omega, t) = -\mathrm{MTR}_{asym}(\Delta\omega, t, P_{z_{eff}} = -\cos\theta) \qquad [34]$$

The pCEST signal can be positive in the transient state, but is negative in the steady state. This inversion recovery approach was suggested first to increase SNR for MT effect by Mangia *et al.* (42) and for SL already by Santyr *et al.* (43) and again by Jin and Kim (44). Their '*iSL*' signal is, in our notation, equal to $Z(\Delta\omega, \omega_1, t)$ (Equation [8]) with $P_{z_{eff}} = -1$ and their projection factors for CEST and SL are identical to P_z and $P_{z_{eff}}$. For R_{ex}, the approximation of ref. (14) is used, assuming $R_{2b} = R_{2a}$. In particular, for the quantification employing different B_1, their approach will benefit from our approximation of R_{ex}. By irradiation with Toggling Inversion Preparation (iTIP), Jin and Kim (44) were able to remove Z^{ss} which allows for the direct exponential fitting of the difference signal of SL and iSL, and thus promises a reduced scanning time.

Separation of R_{ex}

The dependence of CEST and SL on exchange is mediated by R_{ex}, the exchange-dependent relaxation rate in the rotating frame. As the discussed evaluation algorithms for PTR depend on direct water saturation, we propose methods which use the underlying structure of the *Z*-spectrum and yield R_{ex}. For the transient state, QUESTRA can be extended by the inclusion of R_{ex} and the projection factors (in $\tilde{Z}$, Equation [10]):

$$\mathrm{QUESTRA}_{R_{ex}}(t) = \frac{\tilde{Z}(+\Delta\omega, t)}{\tilde{Z}(-\Delta\omega, t)} = e^{-R_{ex}(\Delta\omega)t} \qquad [35]$$

which provides direct access to R_{ex}. The dynamic range can as well be improved experimentally by initial inversion pulses ref. (42) which can modeled by negative Pzeff in Zsnake (Equation [10]). Even without creating $\tilde{Z}$, one can measure the experimental $R_{1\rho}$ $(\Delta\omega)$ decay rate and obtain $R_{ex}(\Delta\omega) \approx R_{1\rho}(+\Delta\omega) - R_{1\rho}(-\Delta\omega)$ by asymmetric analysis of the rate $R_{1\rho}$ $(\Delta\omega)$. For the evaluation of steady-state measurements, we suggest an extension of Equation [30]:

$$\begin{aligned}\mathrm{MTR}_{R_{ex}}(+\Delta\omega) &= \frac{Z^{ss}(-\Delta\omega) - Z^{ss}(+\Delta\omega)}{Z^{ss}(-\Delta\omega)\cdot Z^{ss}(+\Delta\omega)} \\ &= \frac{1}{Z^{ss}(+\Delta\omega)} - \frac{1}{Z^{ss}(-\Delta\omega)} = \frac{R_{ex}(+\Delta\omega)}{\cos\theta \cdot P_z \cdot R_{1a}}\end{aligned} \qquad [36]$$

which yields R_{ex} in units of R_{1a} and is independent of spillover. R_{ex} can be calculated by the determination of R_{1a} and the projection factors. θ can be determined by B_1 mapping and R_{1a} can be measured; however, R_{1a} is not the same as the observed relaxation rate R_{obs} in an inversion or saturation recovery experiment, especially if a macromolecular pool is present (16). As $\mathrm{MTR}_{R_{ex}}$ and $\mathrm{QUESTRA}_{R_{ex}}$ evaluations employ directly *Z*-spectra data, they are useful saturation transfer evaluation methods for the determination of R_{ex} with correction of direct saturation. However, they are still asymmetry based and not applicable to systems with pools with opposed resonance frequencies. In this case, the most reliable evaluation is the fitting of the whole *Z* spectra using Equation [8] including a superimposed R_{ex} of the contributing pools.

Determination of R_{2b}, k_b and f_b

As proposed by Jin *et al.* (12), the width Γ (Equation [18]) of R_{ex} $(\Delta\omega_b)$ can be used to obtain k_b directly. However, especially for small k_b, the extension by R_{2b} is necessary. Fitting R_{ex}^{max} for different B_1 yields f_b and k_b separately, similar to the QUESP method (40) and Dixon's Omega Plots (38), but, again, the neglect of R_{2b} in Equation [19] will distort the values for k_b and f_b. The width of R_{ex} is a linear function of ω_1^2:

$$\frac{\Gamma^2}{4} = \frac{k_b + R_{2b}}{k_b}\cdot\omega_1^2 + (k_b + R_{2b})^2 \qquad [37]$$

and $1/R_{ex}^{max}$ is a linear function of ω_1^{-2}:

$$\frac{1}{R_{ex}^{max}} = \frac{k_b + R_{2b}}{f_b}\cdot\omega_1^{-2} + \frac{1}{f_b k_b} \qquad [38]$$

Hence, fitting of the *Z*-spectra for different B_1 yields f_b, k_b and R_{2b} separately.

CONCLUSION

We extended the analytical solution of the BM equations for SL by the relaxation rate R_{2b} and identified the projection factors necessary for application of the theory to CEST experiments. Temporal evolution, as well as steady-state magnetization of CEST and SL experiments, can be described by one single model governed by the smallest eigenvalue in modulus of the BM equation system, which is $-R_{1\rho}$. $R_{1\rho}$ contains the exchange-dependent relaxation rate R_{ex}. We extended R_{ex} by the transverse relaxation R_{2b}, which allows application of the theory to slow exchange, where R_{2b} is on the order of k_b and not negligible. R_{ex} of different pools can be superimposed to a multi-pool model even for a macromolecular MT pool. Compared with methods designed to estimate PTR, estimators of R_{ex} are less dependent on water proton relaxation. Finally, we showed that the determination of R_{ex} as a function of ω_1 and $\Delta\omega$ allows the determination of the concentration, exchange rate and transverse relaxation of the exchanging pool.

REFERENCES

1. Wolff SD, Balaban RS. NMR imaging of labile proton exchange. J. Magn. Reson. 1990; 86: 164–169.
2. Zhou J, van Zijl PC. Chemical exchange saturation transfer imaging and spectroscopy. Progr. Nucl. Magn. Reson. Spect. 2006; 48: 109–136.
3. Zhou J, Payen J, Wilson DA, Traystman RJ, van Zijl PCM. Using the amide proton signals of intracellular proteins and peptides to detect pH effects in MRI. Nat. Med. 2003; 9: 1085–1090.
4. Cai K, Haris M, Singh A, Kogan F, Greenberg JH, Hariharan H, Detre JA, Reddy R. Magnetic resonance imaging of glutamate. Nat. Med. 2012; 18: 302–306.
5. Jin T, Wang P, Zong X, Kim S. Magnetic resonance imaging of the Amine-Proton EXchange (APEX) dependent contrast. Neuroimage, 2012; 59: 1218–1227.
6. Ling W, Regatte RR, Navon G, Jerschow A. Assessment of glycosaminoglycan concentration in vivo by chemical exchange-dependent saturation transfer (gagCEST). Proc. Natl. Acad. Sci. USA, 2008; 105: 2266–2270.
7. Jia G, Abaza R, Williams JD, Zynger DL, Zhou J, Shah ZK, Patel M, Sammet S, Wei L, Bahnson RR, Knopp MV. Amide proton transfer MR imaging of prostate cancer: a preliminary study. J. Magn. Reson. Imaging, 2011; 33: 647–654.
8. Schmitt B, Zamecnik P, Zaiss M, Rerich E, Schuster L, Bachert P, Schlemmer HP. A new contrast in MR mammography by means of chemical exchange saturation transfer (CEST) imaging at 3 tesla: preliminary results. Fortschr. Roentgenstr. (RoFo) 2011; 183: 1030–1036.
9. Zhou J. Amide proton transfer imaging of the human brain. Meth. Mol. Biol. 2011; 711: 227–237.
10. Gerigk L, Schmitt B, Stieltjes B, Röder F, Essig M, Bock M, Schlemmer HP, Röthke MJ. 7 Tesla imaging of cerebral radiation necrosis after arteriovenous malformations treatment using amide proton transfer (APT) imaging. Magn. Reson. Imaging, 2012; 35: 1207-1209.
11. Schmitt B, Zbyn S, Stelzeneder D, Jellus V, Paul D, Lauer L, Bachert P, Trattnig S. Cartilage quality assessment by using glycosaminoglycan chemical exchange saturation transfer and (23)Na MR imaging at 7 T. Radiology, 2011; 260: 257–264.
12. Jin T, Autio J, Obata T, Kim S. Spin-locking versus chemical exchange saturation transfer MRI for investigating chemical exchange process between water and labile metabolite protons. Magn. Reson. Med. 2011; 65: 1448–1460.
13. Vinogradov E, Soesbe TC, Balschi JA, Sherry AD, Lenkinski RE. pCEST: positive contrast using chemical exchange saturation transfer. J. Magn. Reson. 2011; 215: 64-73.
14. Trott O, Palmer AG. R1ρ relaxation outside of the fast-exchange limit. J. Magn. Reson. 2002; 154: 157–160.
15. Sun PZ, Sorensen AG. Imaging pH using the chemical exchange saturation transfer (CEST) MRI: correction of concomitant RF irradiation effects to quantify CEST MRI for chemical exchange rate and pH. Magn. Reson. Med. 2008; 60: 390–397.

16. Desmond KL, Stanisz GJ. Understanding quantitative pulsed CEST in the presence of MT. Magn. Reson. Med. 2012; 67: 979–990.
17. McConnell HM. Reaction rates by nuclear magnetic resonance. J. Chem. Phys. 1958; 28: 430.
18. Miloushev VZ, Palmer AG III. R1ρ relaxation for two-site chemical exchange: General approximations and some exact solutions. J. Magn. Reson. 2005; 177: 221–227.
19. Trott O, Palmer AG. Theoretical study of R(1ρ) rotating-frame and R2 free-precession relaxation in the presence of n-site chemical exchange. J. Magn. Reson. 2004; 170: 104–112.
20. Moran PR, Hamilton CA. Near-resonance spin-lock contrast. Magn. Reson. Imaging, 1995; 13: 837–846.
21. Woessner DE, Zhang S, Merritt ME, Sherry AD. Numerical solution of the Bloch equations provides insights into the optimum design of PARACEST agents for MRI. Magn. Reson. Med. 2005; 53: 790–799.
22. Stanisz GJ, Odrobina EE, Pun J, Escaravage M, Graham SJ, Bronskill MJ, Henkelman RM. T1, T2 relaxation and magnetization transfer in tissue at 3T. Magn. Reson. Med. 2005; 54: 507–512.
23. Sun PZ, Farrar CT, Sorensen AG. Correction for artifacts induced by B_0(0) and B_1(1) field inhomogeneities in pH-sensitive chemical exchange saturation transfer (CEST) imaging. Magn. Reson. Med. 2007; 58: 1207–1215.
24. Zaiss M, Schmitt B, Bachert P. Quantitative separation of CEST effect from magnetization transfer and spillover effects by Lorentzian-line-fit analysis of z-spectra. J. Magn. Reson. 2011; 211: 149–155.
25. Kim M, Gillen J, Landman BA, Zhou J, van Zijl PCM. Water saturation shift referencing (WASSR) for chemical exchange saturation transfer (CEST) experiments. Magn. Reson. Med. 2009; 61: 1441–1450.
26. Mangia S, Liimatainen T, Garwood M, Michaeli S. Rotating frame relaxation during adiabatic pulses vs. conventional spin lock: simulations and experimental results at 4 T. Magn. Reson. Imaging, 2009; 27: 1074–1087.
27. Michaeli S, Sorce DJ, Idiyatullin D, Ugurbil K, Garwood M. Transverse relaxation in the rotating frame induced by chemical exchange. J. Magn. Reson. 2004; 169: 293–299.
28. Abergel D, Palmer R, Arthur G. A Markov model for relaxation and exchange in NMR spectroscopy. J. Phys. Chem. B, 2005; 109: 4837–4844.
29. Trott O, Abergel D, Palmer AG. An average-magnetization analysis of r 1 relaxation outside of the fast exchange limit. Mol. Phys. 2003; 101: 753–763.
30. Baguet E, Roby C. Off-Resonance irradiation effect in Steady-State NMR saturation transfer. J. Magn. Reson. 1997; 128: 149–160.
31. Longo DL, Dastrù W, Digilio G, Keupp J, Langereis S, Lanzardo S, Prestigio S, Steinbach O, Terreno E, Uggeri F, Aime S. Iopamidol as a responsive MRI-chemical exchange saturation transfer contrast agent for pH mapping of kidneys: In vivo studies in mice at 7 T. Magn. Reson. Med. 2010; 65: 202–211.
32. Schröder L, Lowery TJ, Hilty C, Wemmer DE, Pines A. Molecular imaging using a targeted magnetic resonance hyperpolarized biosensor. Science, 2006; 314: 446–449.
33. Zaiss M, Schnurr M, Bachert P. Analytical solution for the depolarization of hyperpolarized nuclei by chemical exchange saturation transfer between free and encapsulated xenon (HyperCEST). J. Chem. Phys. 2012; 136: 144106-1–144106-10.
34. Schmitt B, Zaiss M, Zhou J, Bachert P. Optimization of pulse train presaturation for CEST imaging in clinical scanners. Magn. Reson. Med. 2011; 65: 1620–1629.
35. Zu Z, Li K, Janve VA, Does MD, Gochberg DF. Optimizing pulsed-chemical exchange saturation transfer imaging sequences. Magn. Reson. Med. 2011; 66: 1100–1108.
36. Sun PZ, Wang E, Cheung JS, Zhang X, Benner T, Sorensen AG. Simulation and optimization of pulsed radio frequency irradiation scheme for chemical exchange saturation transfer (CEST) MRI-demonstration of pH-weighted pulsed-amide proton CEST MRI in an animal model of acute cerebral ischemia. Magn. Reson. Med. 2011; 66: 1042–1048.
37. Zu Z, Janve VA, Li K, Does MD, Gore JC, Gochberg DF. Multiangle ratiometric approach to measure chemical exchange in amide proton transfer imaging. Magn. Reson. Med. 2012; 68: 711–719.
38. Dixon WT, Ren J, Lubag AJM, Ratnakar J, Vinogradov E, Hancu I, Lenkinski RE, Sherry AD. A concentration-independent method to measure exchange rates in PARACEST agents. Magn. Reson. Med. 2010; 63: 625–632.
39. Liu G, Gilad AA, Bulte JWM, van Zijl PCM, McMahon MT. High-throughput screening of chemical exchange saturation transfer MR contrast agents. Contrast Media Mol. Imaging, 2010; 5: 162–170.
40. McMahon MT, Gilad AA, Zhou J, Sun PZ, Bulte JWM, van Zijl PCM. Quantifying exchange rates in chemical exchange saturation transfer agents using the saturation time and saturation power dependencies of the magnetization transfer effect on the magnetic resonance imaging signal (QUEST and QUESP): ph calibration for poly-L-lysine and a starburst dendrimer. Magn. Reson. Med. 2006; 55: 836–847.
41. Sun PZ. Simplified quantification of labile proton concentration-weighted chemical exchange rate (k(ws)) with RF saturation time dependent ratiometric analysis (QUESTRA): normalization of relaxation and RF irradiation spillover effects for improved quantitative chemical exchange saturation transfer (CEST) MRI. Magn. Reson. Med. 2012; 67: 936–942.
42. Mangia S, De Martino F, Liimatainen T, Garwood M, Michaeli S. Magnetization transfer using inversion recovery during off-resonance irradiation. Magn. Reson. Imaging 2011; 29: 1346–1350.
43. Santyr GE, Fairbanks EJ, Kelcz F, Sorenson JA. Off-resonance spin locking for MR imaging. Magn. Reson. Med. 1994; 32: 43–51.
44. Jin T, Kim S-G. Quantitative chemical exchange sensitive MRI using irradiation with toggling inversion preparation. Magn. Reson. Med. 2012; 68: 1056–1064.

APPENDIX A: EIGENVECTOR APPROXIMATION

We consider the Taylor expansion in f_b of the eigenvector $\vec{v}_1$ of the smallest eigenvalue in modulus λ_1. The constant term of this expansion evaluated on the resonance of pool *b* yields for the components of this eigenvector in pool *a*:

$$\vec{v}_1 = \begin{pmatrix} \omega_1 \\ 0 \\ \Delta\omega \end{pmatrix} + \underbrace{\begin{pmatrix} \dfrac{(R_{1a}+\lambda_1)(R_{2a}+\lambda_1)}{\omega_1} \\ \dfrac{\Delta\omega}{\omega_1}(R_{1a}+\lambda_1) \\ 0 \end{pmatrix}}_{*} \qquad [A1]$$

with the approximation of Equation [12], $\lambda_1 = -R_{eff} = R_{1a} + (R_{2a} - R_{1a})sin^2\theta = R_{2a} - (R_{2a} - R_{1a})cos^2\theta$. The first component of (*) can be neglected if:

$$\left|\frac{(R_{1a}-R_{eff})(R_{2a}-R_{eff})}{\omega_1}\right| \ll \omega_1 \qquad [A2]$$

This yields:

$$(R_{2a}-R_{1a})^2 \ll \frac{\omega_1^2}{sin^2\theta cos^2\theta} = \frac{\omega_1^2}{\frac{\omega_1^2\Delta\omega^2}{\omega_{eff}^4}} = \frac{\omega_{eff}^4}{\Delta\omega^2} \qquad [A3]$$

As $\frac{\omega_{eff}^4}{\Delta\omega^2} > \omega_{eff}^2$, this can be reduced to the condition:

$$|R_{2a} - R_{1a}| \ll \omega_{eff} \qquad [A4]$$

The second component of (*) vanishes under the same condition (Equation [A4]). After neglecting (*) and normalizing the eigenvector of the smallest eigenvalue, Equation [A1] simplifies to (Fig. 1a):

$$\vec{v}_1 = \begin{pmatrix} sin\theta \\ 0 \\ cos\theta \end{pmatrix} \qquad [A5]$$

Along this eigenvector, the Bloch–McConnell equations are one-dimensional:

$$\dot{M}_{z_{eff}} = \lambda_1 \cdot M_{z_{eff}} + C_{z_{eff}} \qquad [A6]$$

where the constant part $C_{z_{eff}}$ is the projection of $\vec{C}$ (Equation [3]) on the eigenvector $\vec{v}_1$ (Equation [A5]) giving:

$$C_{z_{eff}} = cos\theta \cdot R_{1a}. \quad [A7]$$

The solution of Equation [A6] is the combination of the general solution of the homogeneous equation (which is an exponential function with rate λ_1) superimposed with a special solution of the inhomogeneous equation. The steady state is a special solution and is obtained by setting $\dot{M}_{z_{eff}} = 0$, which gives:

$$-\lambda_1 \cdot M_{z_{eff}} = cos\theta \cdot R_{1a}. \quad [A8]$$

By backprojection on the z axis and normalization by M_0, we obtain the steady-state solution (Equation [9]):

$$Z^{ss} = \frac{P_z R_{1a} cos\theta}{-\lambda_1} \quad [A9]$$

APPENDIX B: EIGENVALUE APPROXIMATION

The eigenvalues λ_i of an $n \times n$ matrix are the roots of the normalized characteristic polynomial and are defined by:

$$det(\mathbf{A} - \lambda \cdot \mathbf{I}) = 0 \Leftrightarrow \lambda^n + c_{n-1}\lambda^{n-1} + \ldots + c_1\lambda + c_0 = 0 \quad [B1]$$

where:

$$c_0 = (-1)^n det(\mathbf{A}) = (-1)^n \lambda_1 \cdot \ldots \cdot \lambda_n \quad [B2]$$

and:

$$c_1 = (-1)^{n-1} \sum_{i=1}^{n} \frac{\lambda_1 \cdot \ldots \cdot \lambda_n}{\lambda_i} = -c_0 \cdot \sum_{i=1}^{n} \frac{1}{\lambda_i} \quad [B3]$$

The assumption that all eigenvalues are much larger than $|\lambda_1| \ll |\lambda_2| \leq \ldots \leq |\lambda_n|$ leads to:

$$c_1 = -c_0 \cdot \left(\frac{1}{\lambda_1} + \frac{1}{\lambda_2} + \ldots + \frac{1}{\lambda_n} \right) \approx -\frac{c_0}{\lambda_1} \quad [B4]$$

This approximation is also valid for complex eigenvalues, because the conjugate complex is also an eigenvalue, and therefore $\frac{1}{\lambda_j} + \frac{1}{\lambda_j^*} = \frac{2Re(\lambda_j)}{|\lambda_j|2} < \frac{2}{|\lambda_j|}$. Equations [A2] and [A3] allow general approximation of the smallest eigenvalue in modulus by:

$$\lambda_1 = -\frac{c_0}{c_1} \quad [B5]$$

The error is smaller than $\left| \frac{\lambda_1}{\lambda_2 \cdot (n-1)} \right|$. Justified by linearization of the characteristic polynomial, Equation [B5] was also suggested in ref. (14).